Korean J. Chem. Eng., 40(4), 952-963 (2023)
DOI: 10.1007/s11814-022-1244-7

pISSN: 0256-1115
eISSN: 1975-7220

Organic/inorganic nanohybrid of MgAl@$CuFe_2O_4$-polylysine for hazardous Cr(VI) and methyl orange uptake: Multivariate optimization and isotherm study

Hassan Alijani*,†, Mostafa Hossein Beyki, Reyhaneh Kaveh***, and Mojtaba Bagherzadeh*****

*Department of Chemistry, Faculty of Science, Shahid Chamran University of Ahvaz, Ahvaz, Iran
**School of Chemistry, University College of Science, University of Tehran, Tehran, Iran
***Department of Chemistry, Sharif University of Technology, Tehran, Iran, P. O. Box 11155-3615
(*Received 23 May 2022 • Revised 23 July 2022 • Accepted 29 July 2022*)

Abstract−An efficient organic/inorganic magnetic nanohybrid of MgAl@$CuFe_2O_4$-polylysine was successfully synthesized and employed as a suitable adsorbent for removal Cr(VI) and methyl orange from water solution. The prepared nanohybrid was characterized by X-ray diffraction, Fourier transform infrared spectroscopy, scanning electron microscopy, vibrating sample magnetometer and thermogravimetric analysis. The nanohybrid of MgAl@$CuFe_2O_4$-polylysine was employed to adsorb anionic species, i.e., Cr(VI) and methyl orange through electrostatic attraction, ligand exchange and ion exchange. Multivariate optimization with Box-Behnken design was used to evaluate effective parameters such as dosage of adsorbent, solution pH and contact time on adsorption and their interaction. Results showed that pH, contact time and adsorbent dosage are effective parameters for Cr(VI) adsorption; however, the pH of the solution is the sole effective parameter for methyl orange adsorption. Both analyte adsorptions are fast with adsorption times less than 15 min. Isotherm study revealed that the prepared nanohybrid is a highly efficient adsorbent for methyl orange and Cr(VI) with adsorption capacity of 693.6 and 281.8 mg g^{-1}, respectively. Isotherm study showed that adsorption of both analytes well fitted with the Freundlich adsorption isotherm model, which indicated multilayer adsorption on the heterogeneous surface. The magnetic saturation for the prepared adsorbent was 12.64 emu g^{-1}, which was adequate and suitable for magnetic separation of samples. The prepared adsorbent was regenerated using ethanol-aquaeous NaOH solution as it shows 90% removal efficiency after three cycles.

Keywords: Cr(VI), Methyl Orange, Mixed Oxide, Polymer

INTRODUCTION

Surface and groundwater resource contamination is the outcome of industrial development in recent decades. In other words, contaminated water is produced as a result of various human activities in the fields of metallurgy, electroplating, textiles, paper manufacture as well as biomedical activities [1-3]. The hazardous heavy metal and dyes are a constant focus of environmental concern. They are in contaminated water and exert serious pollution risk on the ecological system because of their toxicity and poor biodegradability, which treat humankind's health [4-6]. Among various heavy metals, anionic chromium oxide compounds, i.e., Cr(VI) generally show low solubility and is known to be highly toxic, carcinogenic and epithelial irritant [7-9]. Moreover, methylene orange (MO) as an azo reactive dye in cooperation with aromatic structures has more toxicity to living organisms as if swallowed, it can be fatal [10,11]. Therefore, the stated contents convince researchers to monitor and eliminate heavy metals and dyes from sewage before discharging them into the environment [12]. Up to now, many efforts have been made to develop remediation plans which could eliminate contaminants from wastewater [13]. Coagulation, oxidation, membrane filtration and electrochemical techniques are the most conventional reported methods with high worthiness for water remediation [14]. The mentioned methods show some weaknesses, such as low flexibility of design, being time-consuming, generation of secondary pollution and high operation cost [15,16]. These drawbacks propel the researchers towards the adsorption process as a time-consuming and economical efficient environmental remediation method that requires low technological equipment; moreover, it has the characteristic to be a reusable technique [17-19]. Several adsorbents have been discussed in the literature for removal of heavy metal and dyes, such as MoS_2 [20,21], polymer [22-28], metal oxides [29-31], metal-organic framework [32], graphene oxide [33] and carbon nanotubes [34].

Among various adsorption systems, organic/inorganic hybrid materials possess remarkable characteristics with respect to the pure organic or inorganic fragment since they significantly enhance the mechanical, thermal, optical and physicochemical properties of single-components [35]. Several types of inorganic materials have been employed in polymer composite preparation to improve their performance. Anionic clay or layered double hydroxides (LDHs) is a promising nanofiller in polymer composite preparation [36]. LDHs possess layered hydroxide sheets with intercalated anions along with some water molecules which have high anion exchange capacity [37]. The core of the host LDHs can be incorporated with the polymer chain through in situ polymerization. The organic/inorganic composite shows potential applications in capacitors, sensors, and remediation water in terms of heavy metals and anionic dyes [38,

†To whom correspondence should be addressed.
E-mail: h.alijani@scu.ac.ir

39]. The performance of LDH-polymer in water treatment can be improved through magnetization of it that generates a magnetic hybrid adsorbent as a cheap and highly scalable separation method assisted with an external magnetic field [40-44]. The above-described viewpoints convinced our research group to prepare a magnetic adsorption system for water treatment. Two toxic anionic species, i.e., Cr(VI) and MO, were used as a sample target analyte. As mentioned MgAl LDH was selected as an anion exchange platform to capture the Cr(VI) and MO. In the following, $CuFe_2O_4$ was selected to prepare magnetic LDH. In fact, the magnetic property of composite improved the adsorption properties of adsorbent since it exhibited easy separation. The selected magnetic fragment is a subset of spinel-ceramic ferrites with high corrosive stability and biocompatibility. Finally, the magnetic LDH was strengthened with polylysine as a organic fragment of the hybrid material. The polymer has several hydrophobic backbones that can improve the adsorption behavior of it toward MO. Moreover, additional amin and carboxylic acid functional groups improved chromium adsorption efficiency, as the nanocomposite showed fast adsorption characteristics toward the target analytes. Effective parameters on the adsorption process, including pH, time, and adsorbent dosage, were optimized with response surface methodology (RSM) and an isotherm study was also performed.

EXPERIMENTAL

1. Materials and Instruments

All chemical reagents were supplied from Merck Company (Darmstadt, Germany). Aluminium chloride, magnesium chloride and urea were employed for preparing LDH. $Cu(NO_3)_2$, $FeCl_3 \cdot 4H_2O$ and NaOH were used to prepare magnetic LDH. Methanol, lysine, resorcinol and p- formaldehyde was used to synthesize the polymer nanocomposite. Standard solutions of Cr(VI) with a concentration of 1,000 mg L^{-1}, were prepared with dissolving of $K_2Cr_2O_7$ salt in 0.5 mL of concentrated HNO_3 followed by dilution to appropriate volume with distilled water. A stock solution of MO was prepared by dissolving the desired amount in the appropriate volume of distilled water. The pH was adjusted with 0.1 mol L^{-1} of HNO_3 and 0.1 mol L^{-1} of NH_3.

The morphology of the prepared magnetic polymer composite was characterized at the accelerating voltage of 15 kV with field emission scanning electron microscopy (FE-SEM) using the Sigma VP Zeiss instrument. The magnetic behavior of the composite was studied by vibrating sample magnetometer (VSM, model MDKFD, Iran). The crystallinity of the composite was studied with Cu-Ka (λ=1.540589 Å) radiation in the 2θ range of 2-100° using a powder X-ray diffraction analyzer (Phillips powder diffractometer, X' Pert MPD). Energy dispersive X-ray spectrometry (EDX) was recorded using the Oxford ED-2000 instrument (England). Thermogravimetric analysis (TGA) result was recorded with a TA Q 50. The pH adjustments were performed with a digital pH meter (model 692, metrohm, Herisau, Switzerland). Magnetic separation was assisted with an external magnetic field using a neodymium-iron-boron ($Nd_2Fe_{12}B$) magnet. A Lambda - 25 UV - Vis spectrophotometer was used for recording the absorbance of the MO. A Varian model AA- 400 flame atomic absorption (FAAS) spectrometer (Varian Australia Pty Ltd, Musgrave), equipped with a deuterium lamp background and hollow cathode lamp was used for the determination of Cr(VI). Fourier transform infrared spectra (FT-IR) were measured with Equinox 55 Bruker with the ATR method over the wavelength of 400-4,000 cm^{-1}.

2. Synthesizing LDH and Magnetic Nanocomposite

In a typical synthesis run, 4.0 g of $MgCl_2 \cdot 6H_2O$, 2.36 g of $AlCl_3 \cdot 6H_2O$, and 4.2 g of urea were dissolved in 80 mL methanol by stirring at room temperature for 30 min. The solution was transferred into an autoclave and then kept to 150 °C for 6 h. After cooling to room temperature, the solid white precipitate was collected by centrifugation and washed several times with water and ethanol [45]. Finally, the product was dried at 80 °C for 6 h. For preparing magnetic nanocomposite, 1.0 g of LDH was ultrasonically dispersed in 100 ml of distilled water. After adding 8.0 mmol of Fe^{3+} and 4.0 mmol of Cu^{2+} to it the mixture was stirred at 80 °C for 10 min after increasing the temperature up to boiling state, 4.0 g of NaOH was directly added to the metal ion solution and stirred for 5 min. The obtained product was collected with filter paper, washed with distilled water and dried at 80 °C for 4 h and stored for subsequent application. To prepare polymer nanocomposite, 0.5 g of the magnetic LDH were ultrasonically dispersed in 10 mL distilled water for 10 min. Thereinafter, 0.3 g of lysine in 5 mL distilled water was added to 40 mL ethanol containing 0.3 g of resorcinol. The solution containing monomer was dripped to LDH suspension under ultrasound radiation within 10 min. Then, 0.1 g of p-formaldehyde was added to the suspension and the mixture was refluxed at 70 °C for 24 h. After cooling to room temperature, the product was collected, washed with ethanol and distilled water then, dried at 60 °C for 4 h.

3. Adsorption Procedure

Effective parameters on the adsorption efficiency were optimized by response surface method (RSM) tests using Box-Behnken design (BBD). Design expert 7.0 software was employed and three parameters including pH, contact time and adsorbent dosage were selected as effective parameters. Optimization experiments were performed at 17 designed runs, 5 center points and one block. Sample solutions were 10 mL with the Cr(VI) and MO concentrations of 1 and 5 mg/L, respectively. The values of the parameters are shown in Table 1.

Isotherm data for Cr(VI) and MO was extracted at the optimum value of parameters, including a pH of 2.5 and 6 containing 17 and 19 mg of the nanocomposite and time of 14 and 13 min, respectively. Cr(VI) and MO concentrations were 1-60 and 5-60 mg/L with a volume of 10 mL. After equilibrium, the concentration of the target analytes in the supernatant was determined. The removal percentage (%R) was calculated based on the initial (C_0)

Table 1. Variables of Box-Behnken design

	Parameter	−Level	+Level	−Level	+Level
		Cr	Cr	MO	MO
A	pH	2	7	2	8
B	Time	5	15	5	15
C	Dosage	5	20	5	20

and remaining concentration of the analytes after equilibrium (C_e) using the following equation:

$$\%R = \frac{C_0 - C_e}{C_0} \times 100 \quad (1)$$

RESULTS AND DISCUSSION

1. Characterization

The XRD analysis of magnetic LDH and polymer nanocomposite is shown in Fig. 1(a). The XRD patterns of magnetic Mg-Al showed sharp reflections and clear low intense peaks at low and high 2θ values, which is in good agreement with reflections of LDH [46]. Strong peaks at $2\theta^{o}$ of 11 and 23 corresponding to (003) and (006) faces as the angle of the first peak indicate the interlayer d-spacing of 7.70 Å. The pattern also shows reflections of (012), (015), (018) and (110), which can be indexed to the hexagonal lattice with rhombohedral symmetry [47]. In the XRD pattern scattering at $2\theta^{o}$=28.98°, 32.22°, 36.8°, 42.48°, 57.10°, 62.28° and 74.06°, corresponds to the (220), (311), (222), (400), (422), (511) and (440) crystal plane of the spinel structure of $CuFe_2O_4$ [48]. The appearance of the peaks that is strong and sharp shows magnetic LDH is crystalline perfectly. The polymer nanocomposite exhibited several sharp peaks at $2\theta^{o}$ equal to 10°, 12°, 15°, 20° and 24° which were attributed to the (001), (100), (110) and (111) reflections of the polymer and confirmed that the polymer has good crystallinity. Moreover, observed reflections could be indexed in a pseudo-orthorhombic cell [49]. The crystalline behavior of ferrites is so much affected by the growth of the polymer on its surface. The XRD pattern for the nanocomposite has shown much weaker diffraction peaks due to the high intensity of the polymer on the surface of mixed oxide.

The magnetic property of the composite is depicted as a magnetic hysteresis curve in Fig. 1(b). The curve is based on the magnetization vs. the applied field. According to the results, the magnetic saturation (M_s) for the composite is 12.64 emu g^{-1} which is adequate and suitable for magnetic separation of samples. Decreasing M_s relative to naked magnetic in literature is due to LDH and polymer as a dead magnetic layer. The value of magnetic remanence (M_r) is 0.29, which estimated the superparamagnetic properties of the nanocomposite [50].

The structure of the polymer composite, as well as their func-

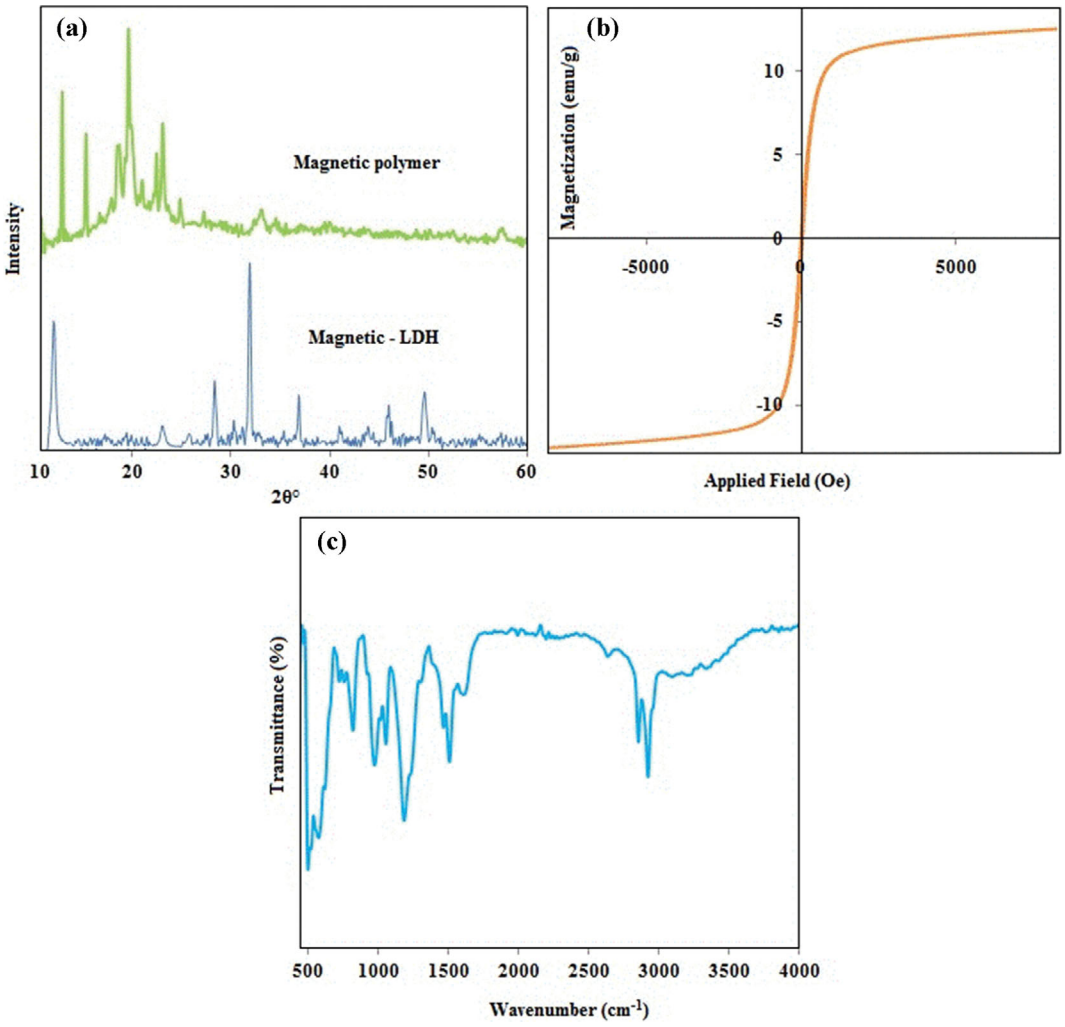

Fig. 1. XRD pattern (a), VSM graph and (b) FTIR spectra (c) of the nanocomposite.

tional groups, was studied using the FT-IR technique and the spectrum is shown in Fig. 1(c). According to the results the peaks corresponding to the Fe-O and Mg-O/Al-O stretching, OH bending vibration, and stretching vibration of residual hydroxyl groups of the $CuFe_2O_4$ and LDH appear at 500-600 cm^{-1}, 1,380-1,390 cm^{-1} and 3,000-3,500 cm^{-1} [51]. Moreover, the characteristic functional groups of polymer show peaks at 2,500-3,500, 2,919, 1,571 and 1,400-1,500 cm^{-1}. The peaks at 2,500-3,500 and 2,919 cm^{-1} correspond to COOH and C-H stretching. Moreover, the peaks at 1,571 and 1,478 cm^{-1} belong to N-H bending units and C=C stretching vibrations of the aromatic ring, respectively [52]. The peaks of C-H out-of-plane bending of the substituted benzenoid ring appear at 800-1,000 cm^{-1} [53].

The FE-SEM image of LDH and polymer nanocomposite is shown in Fig. 2(a) and Fig. 2(b), respectively. According to the image in Fig. 2(a), LDH possesses three-dimensional flake-like structure with a micro-scale in length. It can be seen that the structures were built of alone plates with thicknesses of around 60 nm. The FE-SEM image of magnetic composite (Fig. 2(b)) represents that the surface of the platelets has been covered with polymer, hence they are irregular aggregated structures.

Thermal gravimetric analysis of magnetic LDH and the polymer nanocomposite is shown in Fig. 3(a). The result for magnetic LDH shows that the total weight losses over the temperature range are about 9% due to the solvent evaporation. After polymer synthesis on the surface of the magnetic LDH, the TGA pattern shows total weight losses of 40%; hence, it can be concluded that about 31% of polylysine has been decorated at the magnetic LDH structure. The TGA curve for polymer nanocomposite shows one peak around 200 °C due to the solvent evaporation and another predominant peak around 300-400 °C that can be assighned to the polymer degradation.

Elemental analysis of the magnetic LDH-polylysine composite was performed with the EDX analysis. According to the results in

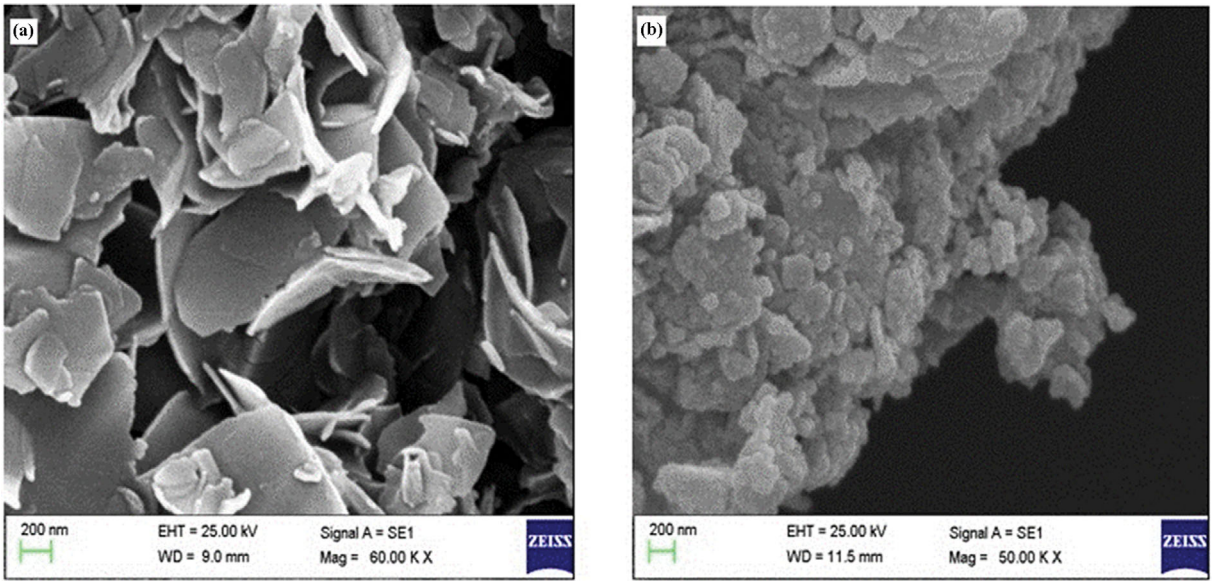

Fig. 2. FESEM image of (a) LDH and (b) magnetic composite.

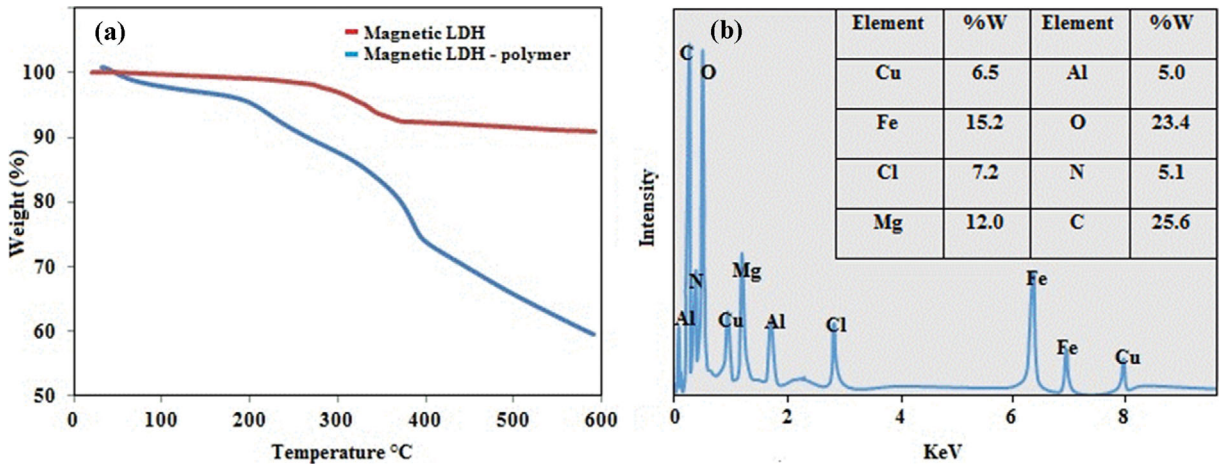

Fig. 3. Thermal gravimetric (a) and EDX pattern (b) of magnetic LDH - polymer nanocomposite.

Fig. 3(b), all initial employed raw elements are observable in the EDX pattern. The Fe and Cu belong to $CuFe_2O_4$; moreover, Mg and Al originated from LDH. The Cl are assigned to the interlayer anion in the LDH structure. The peaks corresponding to the elements of C, O and N are assigned to the polymer fragment of magnetic LDH. This result proves that the nanocomposite preparation was successful.

2. Optimizing Effective Parameters on the Adsorption

To optimize effective parameters of the adsorption process, response surface methodology (RSM) with Box-Behnken design (Design Expert, version 7.0.0) was used. Experiments were performed at 17 runs in one block. About 1.0 mg L^{-1} of Cr(VI) and 5.0 mg L^{-1} of MO with a sample volume of 10 ml were employed to optimize effective parameters. Effective parameters for the adsorption process included pH (A), contact time (B), and adsorbent dose (C). Removal percentage (%R) was used as a response. The polynomial equation for the prediction of response as a function of variables was used [54]:

$$Y = \beta_o + \Sigma_{i=1}^{k}\beta_i X_i + \Sigma_{i=1}^{k}\beta_{ii}X_i^2 + \Sigma_{i=1}^{k-1}\Sigma_{j=2}^{k}\beta_{ij}X_iX_{ij} + \Sigma_{i=1}^{k-1}\Sigma_{j=2}^{k}\beta_{ij}X_i^2X_j \quad (2)$$

In this equation Y and β are the predicted response and regression coefficient constant of the developed model, respectively; also X_i and X_j represent the variable. The relationship between the %R and variable parameters (A, B, and C) for Cr(VI) and MO was obtained in Eqs. (3) and (4), respectively.

$$\text{Removal (\%)} = +87.64 - 5.62A + 1.98B + 1.76C - 3.00\,AB - 5.75AC - 0.77BC - 2.31A^2 + 0.17B^2 - 2.58C^2 \quad (3)$$

$$\text{Removal (\%)} = +82.94 + 16.47A + 1.44B + 1.75C + 7.33AB + 15.25AC + 0.32BC - 51.19A^2 - 3.5B^2 + 1.79C^2 \quad (4)$$

In this equation, A, B and C belong to pH, contact time and sorbent

Table 2. Analysis of variance (ANOVA) for Cr(VI) adsorption

Source	Sum of squares	df	Mean square	F-value	P-value prob>F	
Model	530.47	9	58.94	21.36	0.0003	Significant
A-pH	253.12	1	253.12	91.71	<0.0001	
B-Time	28.50	1	28.50	10.33	0.0148	
C-Dosage	24.85	1	24.85	9.00	0.0199	
AB	36	1	36	13.04	0.0086	
AC	132.25	1	132.25	47.92	0.0002	
BC	2.4	1	2.4	0.87	0.3819	
A^2	22.42	1	22.42	8.12	0.0247	
B^2	0.12	1	0.12	0.043	0.8420	
C^2	28.08	1	28.08	10.17	0.0153	
Residual	19.32	7	2.76			
Lack of fit	8.03	3	2.68	0.95	0.4973	
Pure error	11.29	4	2.82			
Cor total	549.78	16				Not significant

Table 3. Analysis of variance (ANOVA) for MO adsorption

Source	Sum of squares	df	Mean square	F-value	P-value prob>F	
Model	14,560.18	9	1,617.80	103.79	<0.0001	Significant
A-pH	2,169.76	1	2,169.76	139.20	<0.0001	
B-Time	16.59	1	16.59	1.06	0.3366	
C-Dosage	24.61	1	24.61	1.58	0.2493	
AB	214.92	1	214.92	13.79	0.0075	
AC	930.56	1	930.56	59.70	0.0001	
BC	0.41	1	0.41	0.026	0.8758	
A^2	11,034.95	1	11,034.95	707.95	<0.0001	
B^2	51.47	1	51.47	3.30	0.1120	
C^2	13.51	1	13.51	0.87	0.3828	
Residual	109.11	7	15.59			
Lack of fit	15.80	3	5.27	0.23	0.8742	Not significant
Pure error	93.31	4	23.33			
Cor total	14,669.29	16				

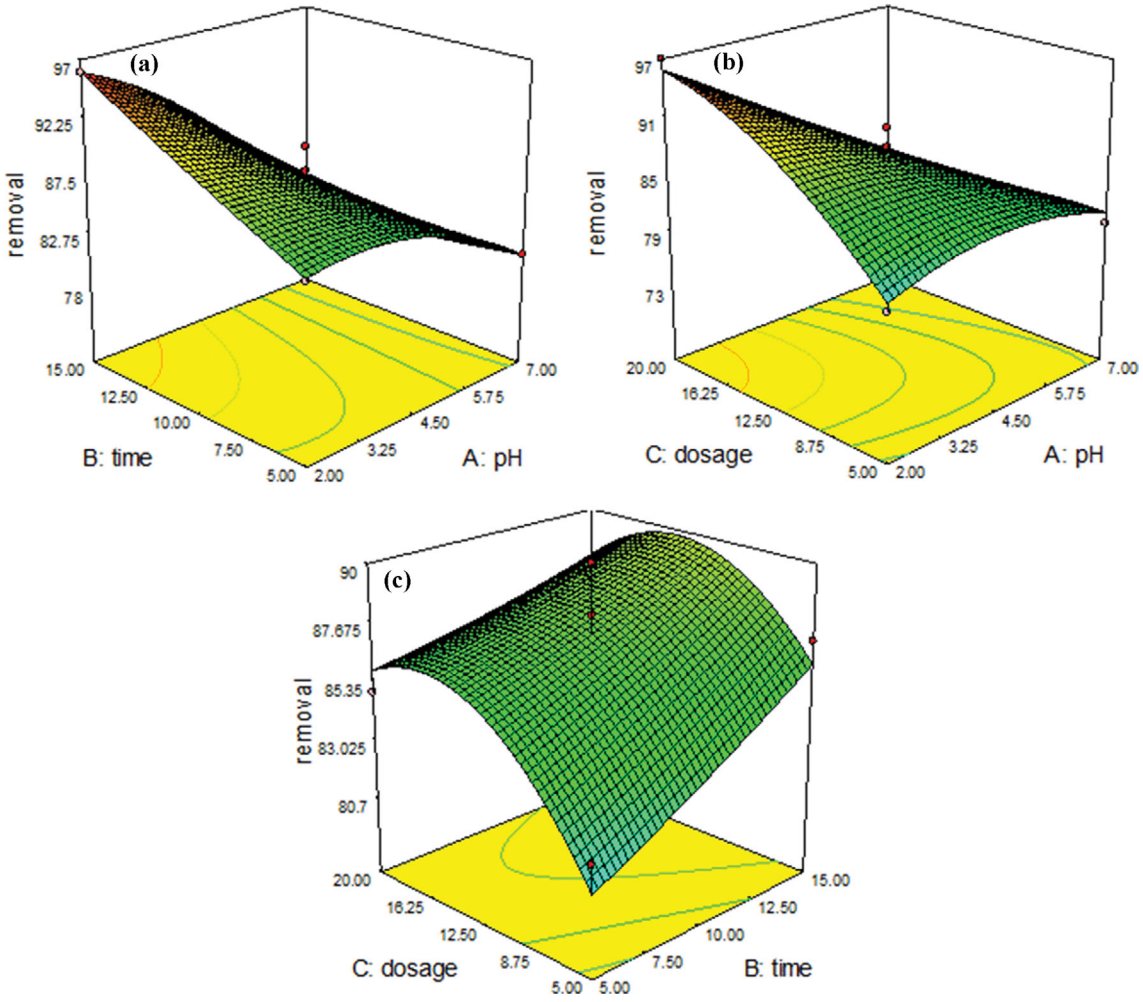

Fig. 4. 3D plot of pH-time (a), pH-adsorbent dosage (b) and adsorbent dosage-time (c) for Cr(VI) adsorption.

dose, respectively. The result of the analysis of variance (ANOVA) is shown in Tables 2 and 3.

The F-value of 21.36 and 103.79 for Cr(VI) and MO imply the model is significant [55]. Values of "Prob>F" less than 0.0003 and 0.0001 indicate model terms are significant. In this case, all three parameters, i.e, pH, time and dosage, are significant terms for Cr(VI) adsorption; however, pH is the sole effective parameter on MO adsorption. The lack of fit F-value of 0.49 and 0.87 implies the Lack of Fit is not significant relative to the pure error. The standard deviation is 1.66 and 3.95 for Cr(VI) and MO adsorption. Adequate precision is 17.95 and 26.80 for Cr(VI) and MO, respectively, while a ratio greater than 4 is desirable.

The results of the 3D plots in the removal of Cr(VI) and MO are shown in Figs. 4 and 5. Based on the results obtained, optimum levels of variables were pH of 2.5 and 6, the adsorbent dosage of 17 and 19 mg and time of 14 and 13 min for Cr(VI) and MO, respectively. Moreover, the normal probability plot (NPP) of the data is represented in Figs. 6(a) and 7(a). The assumptions underlying the analysis are in a straight line with a low violation that confirms the normality of the data. The %R of predicted and experimental values are shown in Figs. 6(b) and 7(b). As can be seen, the percentages of predicted and experimental removal are close, proving excellent experimental work and good consistency. According to the results of the perturbation plot (Figs. 6(c) and 7(c)) removal of Cr(VI) is sensitive to pH, time and dosage. However, MO adsorption is less sensitive to time and adsorbent dosage since the curves show low curvation for these factors. It can be due to the difference between the adsorption mechanisms of the target analytes. Thus, because of the presence of aromatic and methylene groups in the polymer structure, the composite provides several active functional groups that are ready to capture the MO in absence of internal diffusion process. Hence, unlike the Cr(VI) the MO adsorption is less sensitive to time and adsorbent dosage.

3. Adsorption Mechanism

In this work, a composite of magnetic LDH-polylysine has been employed for Cr(VI) and MO adsorption. The composite contains several functional groups, including hydroxyl, carboxyl and amino groups, interlayer anions (Cl^-), methylene groups and aromatic ring [56]. Maximum Cr(VI) adsorption takes place at pH of 2-3. In this situation two main mechanisms iares expected. First is anion exchange between the target anion in the solution and chloride ions in the LDH structure. Electrostatic attraction is the second mechanism in Cr(VI) adsorption by LDH-polymer nanocomposite. Thus, there was electrostatic attraction between $HCr_2O_7^-$-CrO_4^{2-} and elec-

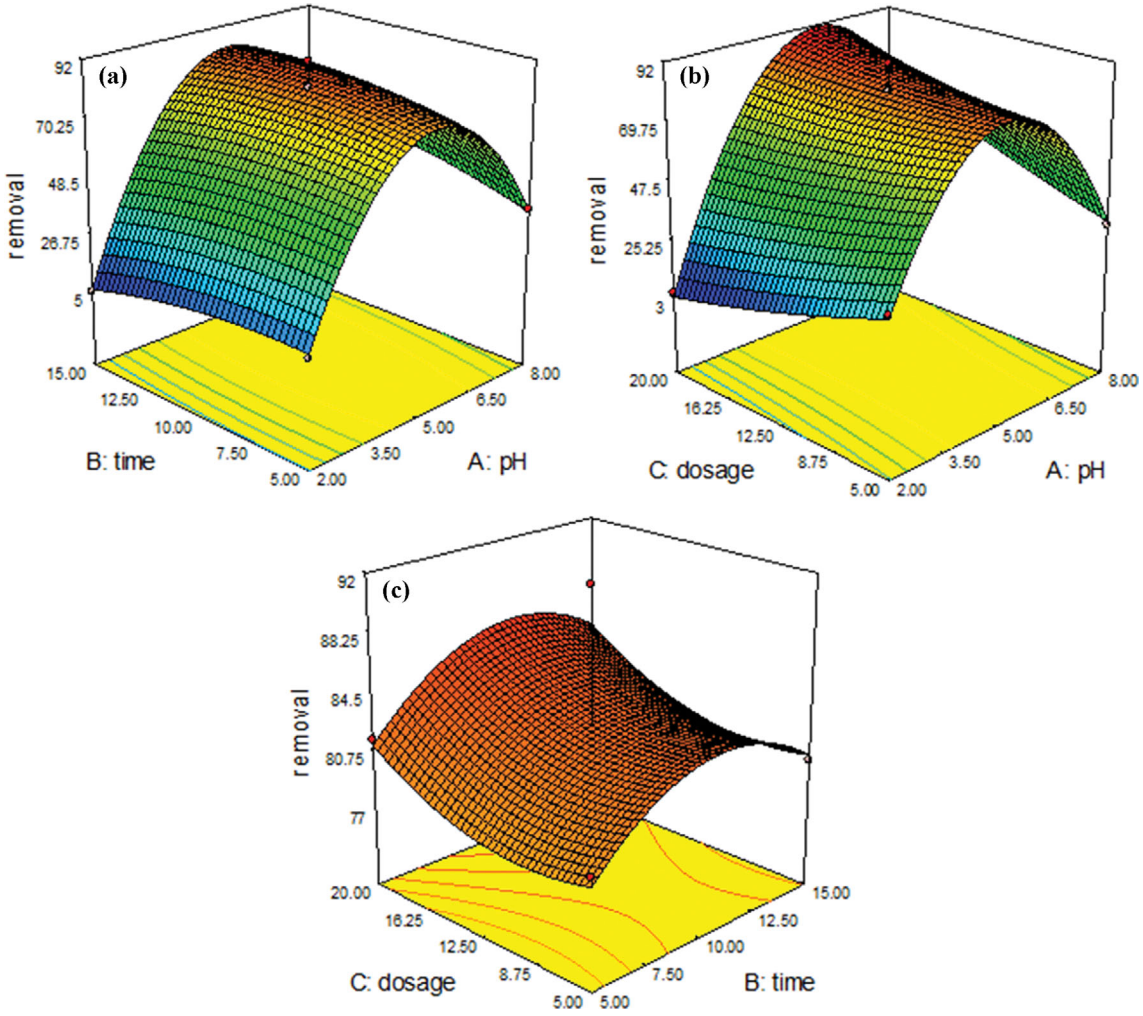

Fig. 5. 3D plot of pH-time (a), pH-adsorbent dosage (b) and adsorbent dosage-time (c) for methyl orange adsorption.

tropositive adsorbent surface since the sorbent contains hydroxyl and amine group, which can be protonated at the working pH. Ligand exchange is another mechanism in chromium adsorption. In the ligand exchange process, the surface hydroxyl groups (M-OH) of LDHs can be exchanged by the adsorbed Cr(VI) through formation of M-O-Cr structure [57]. MO adsorption can take place through electrostatic attraction, hydrogen bonding and hydrophobic interaction. Besides, MO adsorption is less sensitive to time, which confirms the process occurs in absence of internal diffusion. It semms that electrostatic attraction is not dominant since MO adsorption takes place at pH around 6. It seems that hydrophobic and π-π interaction between MO and the composite is the main reason for efficient uptake of it. Benzenoid ring in polymer structure has π electron orbit; moreover, MO containing π electrons can form π-π bonds with each other. Hydrogen bonds because of the NH and OH functional groups on polymer surfaces also participate in MO adsorption as a polar organic chemical [58].

4. Isotherm Study

Two main adsorption isotherm models, Langmuir and Freundlich, were employed to study the effects of Cr(VI) and MO concentrations on the adsorbate-adsorbent interaction. Langmuir's model (Eq. (5)) assumes monolayer coverage at homogeneous sites within the adsorbent [59]. Besides, the Freundlich isotherm (Eq. (6)) model indicates multilayer adsorption on the heterogeneous surface along with the interactions between the adsorbed molecules [60]. The models were described using the nonlinear equations with MATLAB R2013a software. Relative to the linear isotherm model in nonlinear equations the error distribution and isotherm parameters are fixed in the same axis [48]. The model was illustrated with the following equations:

$$Q_e=(bQ_mC_e)/(1+bC_e) \quad (5)$$

$$Q_e=K_fC_e^{1/n} \quad (6)$$

In the above equations, C_e (mg L^{-1}) is the equilibrium concentration of the analyte in the liquid phase, Q_e (mg g^{-1}) is adsorption capacity, and K_f and n are coefficients of the Freundlich model and b and Q_m are Langmuir coefficients [61,62]. Based on the results of the nonlinear Freundlich and Langmuir models (Fig. 8 and Table 4), the R^2 value for Langmuir and Freundlich models is superior to 0.98; hence, the isotherm models were further evaluated by error analysis. As a result, the sum of the squared residual (RSS) was em-

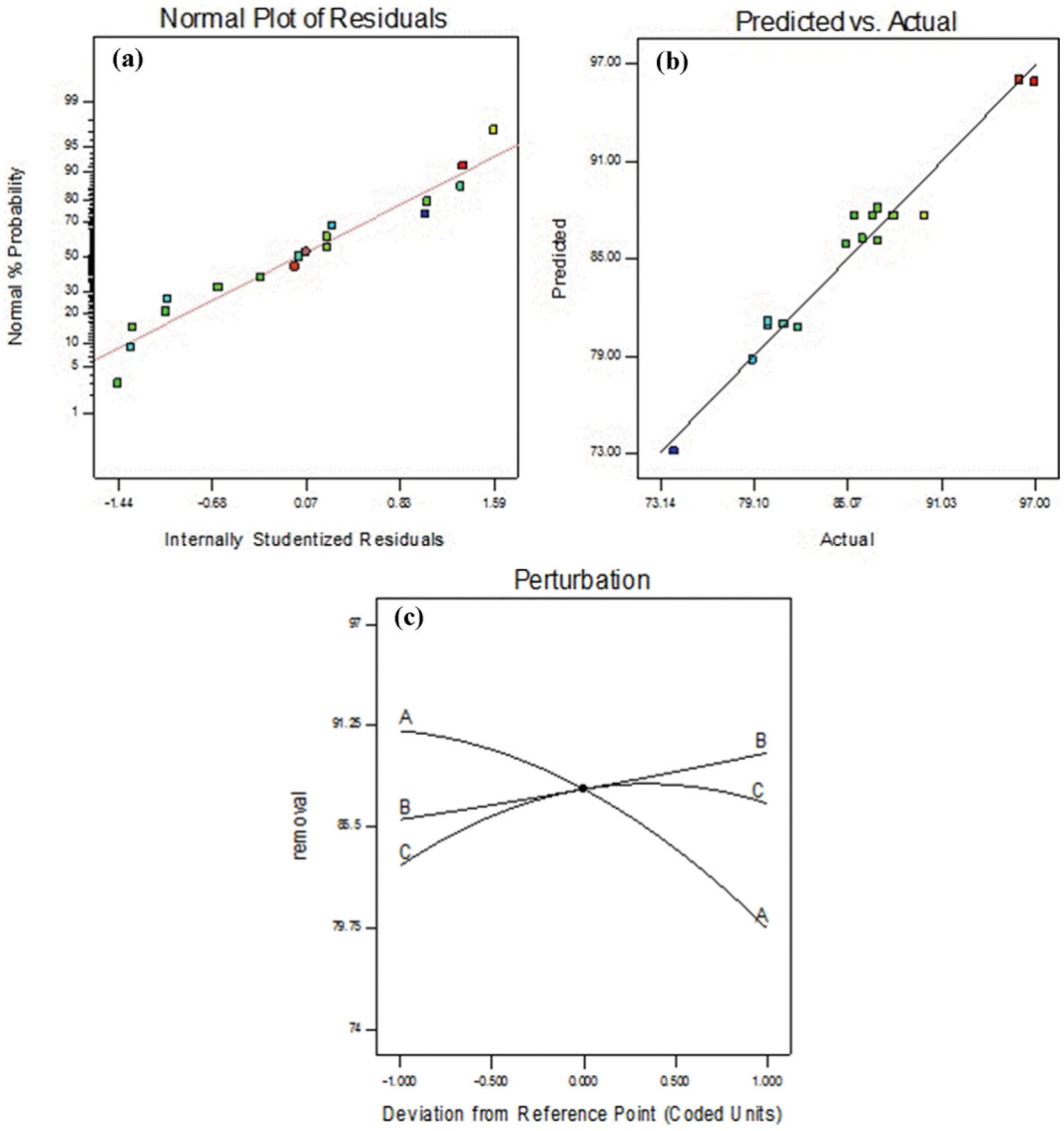

Fig. 6. Normal plot of residuals (a), predicted vs. actual and (b) perturbation plot (c) of Cr(VI) adsorption.

Table 4. The data of isotherm models for MO and Cr(VI) adsorption using magnetic LDH - polymer

Model	Coefficient	MO	Cr(VI)
	Q_m (mg g^{-1})	693.6	281.8
	R^2	0.99	0.98
	b	0.0012	0.0019
Langmuir	RSS	2.4	64.6
	n	0.9	0.96
	K_f	7.8	5.17
Freundlich	R^2	0.99	0.98
	RSS	0.67	58.2

ployed [63]:

$$RSS=\Sigma(Qexp-Qc)^2 \quad (7)$$

where Qexp and Qc are the experimental data, and calculated from the nonlinear model. Moreover, a maximum adsorption capacity of 281.8 and 693.6 mg g^{-1} was obtained for Cr(VI) and MO, respectively. It can be seen from the results in Table 4, the Freundlich model has a lower RSS value relative to the Langmuir model; hence adsorption of Cr(VI) and MO followed the Freundlich model with a multilayer adsorption process. This type of sorption includes direct adsorption of the first layer on the surface of the sorbent along with precipitation or hydrogen bonding type attachment of other layers on the surface of the first layer [64-66].

5. Desorption and Reusability

Regeneration of the sorbent is a main factor that makes the sorption process more economical. According to the effect of pH on Cr(VI) and MO removal, adsorption was not feasible at pH higher than 6; moreover, both analytes are anionic species that can adsorb onto adsorbent through an anion exchange mechanism, so it may be estimated that alkali solution is feasible to release adsorbed dye and Cr(VI). To release MO, ethanol-aqueous NaOH solution (1.0 mol L^{-1}) was tested. Obtained results indicated that more than 95%

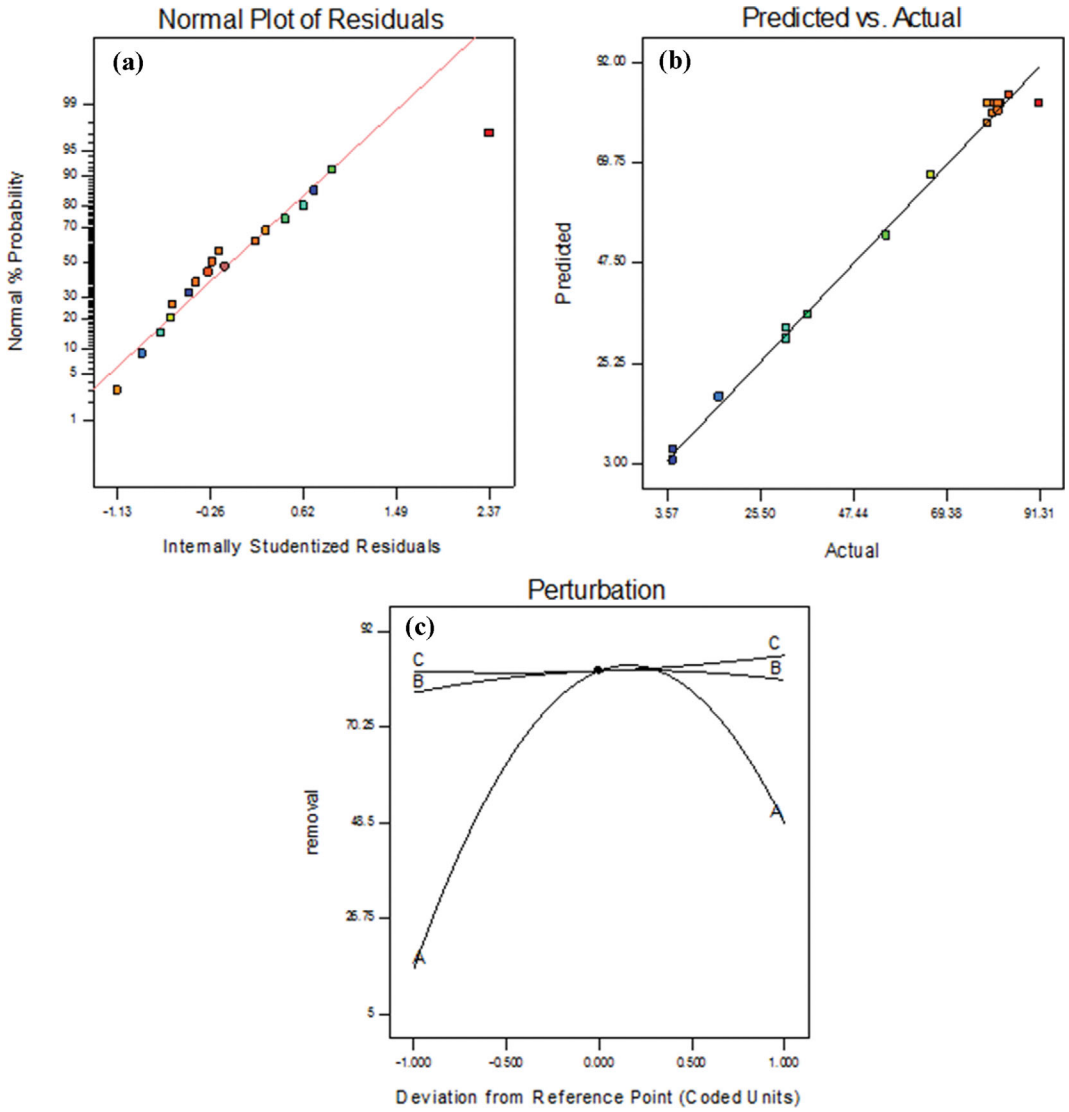

Fig. 7. Normal plot of residuals (a), predicted vs. actual, (b) and perturbation plot (c) of methyl orange adsorption.

Table 5. Comparison of the Cr(VI) adsorption property of prepared composite with some sorbents

Adsorbent	Cr(VI)		Ref
	Q_m (mg g^{-1})	Time (min)	
Iron - zirconium oxide	59.88	60	[15]
Polyethylenimine- poly(vinyl alcohol) -Fe_3O_4	88.4	8	[17]
[1]CS-MWNT-PAA-PADPA/FG	2000	60	[18]
Ionic liquid/polymer	66.1	10	[24]
Graphene oxide/Fe_3O_4	180.8	12 h	[33]
Cellulose/polyaniline	38.76	20	[28]
Polypyrrole/maghemite	209	60	[44]
MgAl@$CuFe_2O_4$ - polymer	281.8	14	This work

[1]Chitosan (CS) based functional gel (FG), multiwall carbon nanotube (MWNT)-poly(acrylic acid) (PAA)-poly(4-amino diphenyl amine) (PADPA).

of adsorbed dye had been released. Moreover, 1.0 mol L^{-1} of aqueous NaOH solution can release more than 98% of Cr(VI). Therefore, ethanol-aqueous NaOH and aqueous NaOH solution was selected as an effective one for the release of MO and Cr(VI), respectively. To evaluate the reusability of the sorbent it was loaded with the target analytes with initial concentration of 5 mg/L for three cycles and desorption was performed. It was found that the removal efficiency was more than 95% at first cycle and reached to around

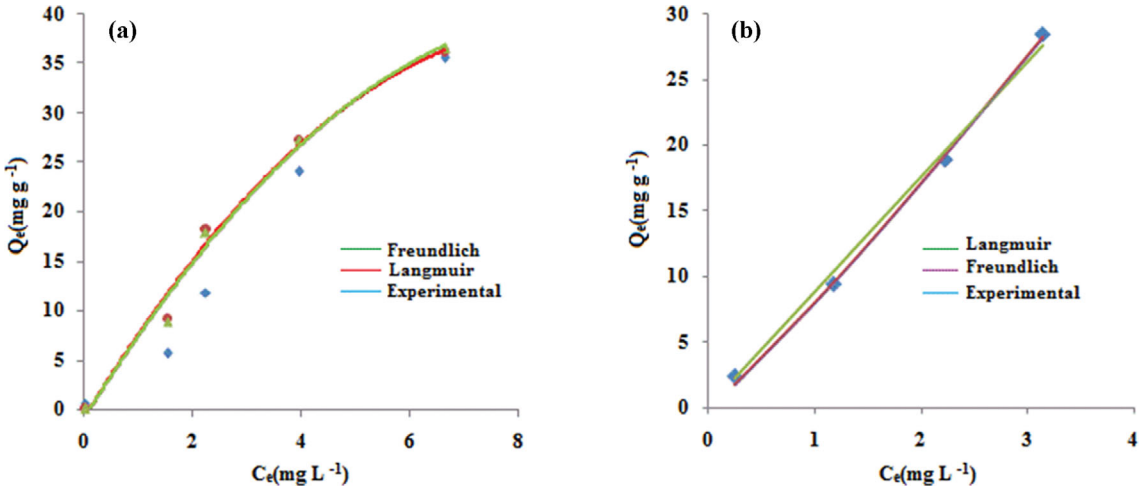

Fig. 8. Nonlinear isotherm plot of Cr(VI) (a) and methylene orange (b) adsorption.

Table 6. Comparison of the MO adsorption property of prepared composite with some sorbents

Adsorbent	MO		Ref
	Q_m (mg g^{-1})	Time (min)	
Lead oxide - activated carbon	333.33	30	[10]
Ammonium - silica	105.4	10	[12]
Modified ostrich bone	573.6	50	[13]
Mesoporous carbon	294.1	60	[14]
[1]Poly(AM - DADMAC)/silica sol	31.3	30	[22]
Chitosan/maghemite	779	300	[40]
Fe_3O_4/activated carbon-HNO_3	303.03	180	[43]
MgAl@$CuFe_2O_4$ - polymer	693.6	13	This work

[1]Acrylamide (AM), diallyl dimethyl ammonium chloride (DADMAC).

92 and 90% in second and third cycle. It can be concluded that the nanocomposite has good efficiency as a reusable sorbent for water treatment.

6. Comparison with other Methods

The MO and Cr(VI) adsorption efficiency of the presented sorbent was compared with some reports in the literature in Tables 5 and 6. The performance of the prepared sorbents is appropriate concerning adsorption time as followed by fast adsorption kinetic. Moreover, they demonstrate satisfactory sorption capacities which are higher than the values for most reported adsorbents. These results indicate that the presented method is a promising route for the removal of anionic species from aqueous solutions.

CONCLUSIONS

The present work was used to develop an efficient adsorption route for the removal of Cr(VI) and methyl orange from aqueous solutions. MgAl@$CuFe_2O_4$ magnetic layered double hydroxide was synthesized by facial precipitation route and employed to prepare polylysine derivative nanocomposite. The adsorption process showed a fast equilibrium time of less than 15 min with good adsorption properties. The response surface method was used to optimize the effective parameters of the adsorption process. Results showed that solution pH is an effective factor in MO adsorption, besides solution pH, contact time and adsorbent dosage are important parameters on Cr(VI) removal. Based on the environmental remediation performance, the mixed oxide - polymer composite exhibited good efficiency for removing anionic species, i.e., hazardous azo dye and Cr(VI) from an aqueous solution.

ACKNOWLEDGEMENTS

The authors thank the Iranian National Science Foundation (grant INSF 99017447), Research Council of the University of Tehran, Shahid Chamran University of Ahvaz and Sharif University of Technology for financial support.

REFERENCES

1. J. Tian, G. Li, W. He, K. Tan, D. Sun, J. Wei and Q. Li, *Chin. J. Chem. Eng.*, In press (2022), Doi:10.1016/j.cjche.2021.12.029.
2. L. Hu, S. Tao, J. Xian, X. Zhang, Y. Liu, X. Zheng and X. Lin, *Chin. J. Chem. Eng.*, **43**, 230 (2022).
3. R. Kaveh and M. Bagherzadeh, *Diam. Relat. Mater.*, **124**, 108923 (2022).
4. L. Zeng, M. Xie, Q. Zhang, Y. Kang, X. Guo, H. Xiao, Y. Peng and

J. Luo, *Carbohydr. Polym*., **123**, 89 (2015).
5. Y. Wang, G. Xia, C. Wu, J. Sun and W. Huang, *Carbohydr. Polym*., **115**, 686 (2015).
6. P. Zhang, Q. An, J. Guo and C. Wang, *J. Colloid Interface Sci*., **389**, 10 (2013).
7. A. B. Albadarin, C. Mangwandi, A. Al-Muhtaseb, G. Walker, S. Allen and M. N. M. Ahmad, *Chin. J. Chem. Eng*., **20**, 469 (2012).
8. Q. Wang, Y. Guan, X. Liu, M. Yang and X. Ren, *Chin. J. Chem. Eng*., **20**, 105 (2012).
9. R. Kaveh, H. Alijani and M. Hossein Beyki, *Polym. Bull.*, **77**, 1893 (2020).
10. M. Bagherzadeh and R. kaveh, *Photochem. Photobiol.*, **94**, 1210 (2018).
11. B. Zhao, X. Sun, L. Wang, L. Zhao, Z. Zhang and J. Li, *Chin. J. Chem. Eng*., **27**, 1973 (2019).
12. J. Liu, S. Ma and L. Zang, *Appl. Surf. Sci*., **265**, 393 (2013).
13. M. Arshadi, A. R. Faraji, M. J. Amiri, M. Mehravar and A. Gil, *J. Colloid Interface Sci*., **446**, 11 (2015).
14. N. Mohammadi, H. Khani, V. Kumar, E. Amereh and S. Agarwal, *J. Colloid Interface Sci*., **362**, 457 (2011).
15. Y. Wang, D. Liu, J. Lu and J. Huang, *Colloids Surf. A Physicochem. Eng. Asp*., **481**, 133 (2015).
16. C. Chen, S. Yao, H. Peng, C. Zeng and H. Song, *J. Eng. Appl.*, **18**, 59 (2015).
17. X. Sun, L. Yang, Q. Li, Z. Liu, T. Dong and H. Liu, *Chem. Eng. J.*, **262**, 101 (2015).
18. M. K. Kim, K. S. Sundaram, G. A. Iyengar and K. PL, *Chem. Eng. J.*, **267**, 51 (2015).
19. E. M. S. Azzam, A. F. M. El-Farargy, M. A. Hegazy and A. A. El-Aal, *J. Dispers. Sci. Technol*., **35**, 175 (2014).
20. L. Ye, H. Xu, D. Zhang and S. Chen, *Mater. Res. Bull*., **55**, 221 (2014).
21. M. J. Aghagoli, M. Hossein Beyki and F. Shemirani, *Food Chem*., **223**, 8 (2017).
22. X. Yang and L. Ni, *Chem. Eng. J.*, **209**, 194 (2012).
23. H. A. Panahi, M. Nikpour, R. A. K. Nezhati and E. Moniri, *Korean J. Chem. Eng*., **30**, 1722 (2013).
24. Y. Jiang, F. Li, G. Ding, Y. Chen, Y. Liu, Y. Hong, P. Liu, X. Qi and L. Ni, *J. Colloid Interface Sci*., **455**, 125 (2015).
25. A. Kiani and M. Ghorbani, *J. Dispers. Sci. Technol.*, **38**, 1041 (2017).
26. C. Albertina, A. Debrassi, J. Dal, N. Nedelko, A. Ślawska-Waniewska, P. Dłużewski, J. Greneche and C. Antonio Rodrigues, *J. Water Process. Eng*., **7**, 141 (2015).
27. M. Hossein Beyki, M. Bayat and F. Shemirani, *Bioresour. Technol*., **218**, 326 (2016).
28. B. Qiu, C. Xu, D. Sun, Q. Wang, H. Gu, X. Zhang, B. L. Weeks, J. Hopper, T. C. Ho, Z. Guo and S. Wei, *Appl. Surf. Sci*., **334**, 7 (2015).
29. J. Rong, T. Zhang, F. Qiu and M. Chen, *Korean J. Chem. Eng*., **32**, 1 (2016).
30. X. Wang, Y. Chen, W. Zhang, W. He, J. Wang and B. Chen, *Korean J. Chem. Eng*., **32**, 1 (2015).
31. X. Ge, H. Hu, C. Deng, Q. Zheng, M. Wang and G. Chen, *Mater. Lett*., **141**, 214 (2015).
32. E. Haque, J. W. Jun and S. H. Jhung, *J. Hazard. Mater*., **185**, 507 (2011).
33. H. Wang, X. Yuan, Y. Wu, X. Chen, L. Leng, H. Wang, H. Li and G. Zeng, *Chem. Eng. J*., **262**, 597 (2015).
34. Y. Yao, B. He, F. Xu and X. Chen, *Chem. Eng. J*., **170**, 82 (2011).
35. S. S. Ray, P. Maiti, M. Okamoto, K. Yamada and K. Ueda, *Macromolecules*, **35**, 3104 (2002).
36. A. M. Alansi, W. Z. Alkayali, M. H. Al-qunaibit, T. F. Qahtan and T. A. Saleh, *RSC Adv*., **5**, 71441 (2015).
37. H. Zaghouane-boudiaf, M. Boutahala and L. Arab, *Chem. Eng. J*., **187**, 142 (2012).
38. B. J. Kim, S. G. Oh, M. G. Han and S. S. Im, *Langmuir*, **16**, 5841 (2000).
39. F. R. Costa, A. Leuteritz, U. Wagenknecht, D. Jehnichen, L. Häußler and G. Heinrich, *Appl. Clay Sci*., **38**, 153 (2008).
40. L. Obeid, A. Bée, D. Talbot, S. Ben Jaafar, V. Dupuis, S. Abramson, V. Cabuil and M. Welschbillig, *J. Colloid Interface Sci*., **410**, 52 (2013).
41. M. J. Pirouz, M. Hossein Beyki and F. Shemirani, *Food Chem*., **170**, 131 (2015).
42. X. Ge, C. D. Gu, X. L. Wang and J. P. Tu, *J. Colloid Interface Sci*., **45**, 134 (2015).
43. M. Huy, N. Hoa, T. Dung, T. T. S. Pham, V. K. Nguyen, T. T. T. Vu, T. Kim and P. Nguyen, *Chemosphere*, **85**, 1269 (2011).
44. A. E. Chávez-guajardo, J. C. Medina-llamas, L. Maqueira, C. A. S. Andrade, K. G. B. Alves and C. P. Melo, *Chem. Eng. J*., **281**, 826 (2015).
45. P. P. Huang, C. Y. Cao, F. Wei, Y. B. Sun and W. G. Song, *RSC Adv*., **5**, 10412 (2015).
46. K. Yang, L. G. Yan, Y. M. Yang, S. J. Yu, R. Shan, H. Yu, B. Zhu and B. Du, *Sep. Purif. Technol*., **124**, 36 (2014).
47. J. Zhou, S. Yang, J. Yu and Z. Shu, *J. Hazard. Mater*., **192**, 1114 (2011).
48. M. Hossein Beyki, M. Mohammadirad, F. Shemirani and A. A. Saboury, *Carbohydr. Polym*., **157**, 438 (2017).
49. J. P. Pouget, M. E. Jozefowicz, A. J. Epstein, X. Tang and A. G. MacDiarmid, *Macromolecules*, **24**, 779 (1991).
50. J. Nonkumwong, P. Pakawanit, A. Wipatanawin, P. Jantaratana, S. Ananta and L. Srisombat, *Mater. Sci. Eng. C*., **61**, 123 (2016).
51. B. Sahoo, S. K. Sahu, S. Nayak, D. Dhara and P. Pramanik, *Catal. Sci. Technol*., **2**, 1367 (2012).
52. M. Khairy and M. F. Gouda, *J. Adv. Res*., **6**, 555 (2014).
53. S. H. Hosseini and A. Asadnia, *J. Nanomater*., **2012**, 1 (2012).
54. S. Jorfi, R. Darvishi Cheshmeh Soltani, M. Ahmadi, A. Khataee and M. Safari, *Environ. Manag. Today*, **187**, 111 (2017).
55. A. M. Bandpei, S. M. Mohseni, A. Sheikhmohammadi, M. Sardar, M. Sarkhosh, M. Almasian, M. Avazpour, Z. Mosallanejad, Z. Atafar, S. Nazari and S. Rezaei, *Korean J. Chem. Eng*., **32**, 1 (2015).
56. L. G. Yan, Y. Y. Xu, H. Q. Yu, X. Xin, Q. Wei and B. Du, *J. Hazard. Mater*., **179**, 244 (2010).
57. Y. Xue, H. Hou and S. Zhu, *J. Hazard. Mater*., **162**, 973 (2009).
58. M. Hossein Beyki, F. Feizi and F. Shemirani, *React. Funct. Polym*., **103**, 81 (2016).
59. Z. Dong, H. Xu, Z. Bai, H. Wang, L. Zhang, X. Luo, Z. Tang, R. Luquec and J. Xuan, *RSC Adv*., **5**, 78352 (2015).
60. Q. Xin, J. Fu, Z. Chen, S. Liu, Y. Yan, J. Zhang and Q. Xu, *J. Environ. Chem. Eng*., **3**, 1637 (2015).
61. R. Kaveh, H. Alijani, M. Hossein Beyki and M. Jafari Pirouz, *Desalin Water Treat*., **212**, 376 (2021).
62. F. Q. An, R. Y. Wu, M. Li, T. P. Hu, J. F. Gao and Z. G. Yuan, *React. Funct. Polym*., **118**, 42 (2017).

63. R. Kaveh, H. Alijani and M. Hossein Beyki, *Polym. Bull.*, **77**, 1893 (2020).
64. K. V. Kumar, *J. Hazard. Mater.*, **137**, 1538 (2006).
65. Q. Li, Z. Wang, D. Fang, H. Y. Qu, Y. Zhu, H. J. Zou, Y. R. Chen, Y. P. Du and H. L. Hu, *New J. Chem.*, **123**, 248 (2014).
66. J. Zhou, Y. Liu, X. Zhou, J. Ren and C. Zhong, *J. Colloid Interface Sci.*, **507**, 107 (2017).